OXFORD GENETICS

GENETICS, 2021, 218(1), iyab041
DOI: 10.1093/genetics/iyab041
Advance Access Publication Date: 13 March 2021
Investigation
Highlighted Article

A novel allele of *SIR2* reveals a heritable intermediate state of gene silencing

Delaney Farris,† Daniel S. Saxton ,† and Jasper Rine*

Department of Molecular and Cell Biology, University of California, Berkeley, CA 94720, USA
†These authors are co-first authors.

*Corresponding author: jrine@berkeley.edu

Abstract

Genetic information acquires additional meaning through epigenetic regulation, the process by which genetically identical cells can exhibit heritable differences in gene expression and phenotype. Inheritance of epigenetic information is a critical step in maintaining cellular identity and organismal health. In *Saccharomyces cerevisiae*, one form of epigenetic regulation is the transcriptional silencing of two mating-type loci, *HML* and *HMR*, by the SIR-protein complex. To focus on the epigenetic dimension of this gene regulation, we conducted a forward mutagenesis screen to identify mutants exhibiting an epigenetic or metastable silencing defect. We utilized fluorescent reporters at *HML* and *HMR*, and screened yeast colonies for epigenetic silencing defects. We uncovered numerous independent *sir1* alleles, a gene known to be required for stable epigenetic inheritance. More interestingly, we recovered a missense mutation within *SIR2*, which encodes a highly conserved histone deacetylase. In contrast to *sir1*Δ, which exhibits states that are either fully silenced or fully expressed, this *sir2* allele exhibited heritable states that were either fully silenced or expressed at an intermediate level. The heritable nature of this unique silencing defect was influenced by, but not completely dependent on, changes in rDNA copy number. Therefore, this study revealed a heritable state of intermediate silencing and linked this state to a central silencing factor, Sir2.

Keywords: epigenetic inheritance; Sir2; transcriptional silencing

Introduction

Transcriptional gene silencing is critical for proper cellular function, differentiation, and development. A temporally coordinated program of changing chromatin environments maintains cell fate by altering gene expression. Consequently, aberrant gene silencing and expression can lead to a variety of disease states (reviewed in Lee and Young 2013). A better understanding of how transcriptional silencing is maintained over time and remembered through cellular division is therefore crucial to understanding its misregulation.

One context in which transcriptional silencing has been studied in detail is the single-celled eukaryote *Saccharomyces cerevisiae*. *Saccharomyces cerevisiae* exhibits stable, epigenetic silencing of transcription through the action of the SIR complex, which produces heterochromatin-like repressive chromatin domains (Kueng *et al.* 2013; Gartenberg and Smith 2016). This budding yeast has two mating types, *a* and α, with mating-type-specific information expressed from the two alleles of the *MAT* locus on Chromosome III. Two loci that undergo stable silencing are the silent mating-type loci, *HML* and *HMR*. These extra copies of mating-type information are distal to the expressed *MAT* locus and allow for mating-type switches in the subset of strains with the *HO* gene, which encodes a site-specific nuclease that cuts at *MAT* (Kostriken *et al.* 1983).

HML and *HMR* are stably repressed, making mating-type solely dependent on the allele of the *MAT* locus. Mutations in *SIR2*, *SIR3*, or *SIR4*, which collectively encode the SIR complex, result in complete loss of silencing at *HML* and *HMR* (Rine and Herskowitz 1987). The SIR complex is recruited to silencer elements within *HML* and *HMR*, deacetylates histones via the catalytic activity of Sir2, and binds to nucleosomes throughout the locus, resulting in transcriptional repression (Hoppe *et al.* 2002; Rusché *et al.* 2002; Thurtle and Rine 2014). Though Sir2, Sir3, and Sir4 are necessary for *HML* and *HMR* silencing, Sir1 was identified by mutant alleles that produced only partial loss of silencing at these loci (Rine *et al.* 1979). Characterization of the *sir1* phenotype at the single-cell level revealed that the expression states of *HML* and *HMR* are bistable in the absence of Sir1 (Pillus and Rine 1989). Quantitative RNA FISH studies show that in the silenced fraction of a *sir1*Δ population, *HML* and *HMR* are as fully silenced as in *SIR*$^+$ cells (Dodson and Rine 2015). Likewise, in the unsilenced fraction, *HML* and *HMR* are as expressed as in *sir2*Δ, *sir3*Δ, or *sir4*Δ mutants. These two expression states in *sir1*Δ are also heritable, as the mother cell's expression state can be passed on faithfully to daughter cells for multiple generations, with switches to the opposite expression state occurring at a low rate.

In *sir1*Δ mutants, some cells manage to heritably silence *HML* and *HMR*, while others exhibit derepression of these loci. One possible explanation for the partial loss of silencing would be the existence of another gene with an overlapping function with *SIR1*; the absence of both factors would then be necessary to observe full derepression. Screens for enhancers of the *sir1*Δ

Received: December 11, 2020. **Accepted:** March 08, 2021

silencing defect have largely uncovered more alleles of *SIR2*, *SIR3*, and *SIR4* (Stone *et al.* 2000). Screens for multicopy suppressors of the silencing defect of *sir1Δ* mutants recovered *HTZ1*, which encodes a variant of histone H2A, and *ESC2* (Dhillon and Kamakaka 2000). However, unlike *sir1Δ*, *htz1* and *esc2* do not exhibit a bistable phenotype. Therefore, mutants that function similarly to *sir1Δ* have eluded previous studies.

A screen to identify bistable silencing mutants has not previously been reported, nor have any reports appeared of heritable intermediate levels of gene silencing. In this study, we carried out a forward mutagenesis screen to identify metastable silencing mutants in *S. cerevisiae*. This screen differed from past screens in the use of fluorescent reporter genes at *HML* and *HMR*, providing the opportunity to observe silencing and heritability quantitatively at both the population and single-cell level.

Materials and methods

Strains and culture methods

All strains were derived from W303 and are listed in the Supplementary Table S1. Plasmids used in the study are listed in Supplementary Table S2. All oligonucleotides, used for cloning, PCR, and sequencing, are listed in Supplementary Table S3. Strains were grown in Yeast Peptone Dextrose (YPD), or Complete Supplement Mixture (CSM) with or without individual amino acids left out (Sunrise Science Products), as indicated. The FLuorescent Analysis of Metastable Expression (FLAME) reporter strain was initially published in Saxton and Rine (2019). Throughout this study, there were subtle differences between the silencing levels of *HML* versus *HMR*; however, the expression phenotypes of both remained similar. Elucidating any differences between the two loci was not pursued further. Mutagenesis was induced with Ethyl Methane Sulfonate (EMS). Diploid strains were created by genetic crosses and phenotypes were confirmed following sporulation by tetrad analysis. The point mutations within *SIR1* and *SIR2* were identified by PCR amplification and sequencing. Each mutant generated by mutagenesis was expected to contain multiple base-pair substitutions. Strains with single point mutations in the genes of interest were engineered using Cas9 technology, as previously described (Lee *et al.* 2015; Brothers and Rine 2019). Single guide RNAs (sgRNAs) targeting *SIR2* and a unique linker region in *sir1Δ::LEU2* (JRY12861) are listed in Supplementary Table S3. To generate *sir1* alleles in an unmutagenized parent strain, PCR-amplified repair templates of sequence-confirmed *sir1* alleles replaced the *sir1Δ::LEU2* allele in JRY12861. To create *sir2-G436D* in an unmutagenized parent strain, *sir2-G436D* was PCR amplified from JRY12466 and provided as a repair template to replace the *SIR2* allele in JRY12860. Both *sir1* and *sir2-G436D* mutant allele integration replaced the Cas9-directed cut site. All single point mutations were sequence confirmed. The Sir2-3xV5 fusion protein used for immunoblotting was created as described (Longtine *et al.* 1998). Strains were transformed with an amplified fragment of pJR3190 (Bähler *et al.* 1998), which allowed for homologous recombination and integration of the *KanMX* cassette and the 3x-V5 tag to the carboxyl terminus of the *SIR2* open reading frame. *SIR2* and *sir2-G436D* were amplified from JRY12860 and JRY12564, respectively, with 300 base pairs of 5′ promoter sequence and 200 base pairs of 3′ terminator sequence. These fragments were integrated into the 2-micron plasmid vector pRS426 to generate pJR3523 and pJR3524. *fob1Δ::KanMX* was generated by amplification of *KanMX* from pJR3190 and subsequent transformation. To test rDNA recombination rates, *yEGFP::K.lac.URA3* was integrated into *RDN37*.

EMS mutagenesis

The EMS protocol was adapted from previously reported protocols (Winston 2008; Liu and Hu 2010) and optimized for our reporter strain (JRY12860) and reagents to yield ∼50–60% lethality. Cells were plated at a low density (∼150–200 colonies) on YPD for screening. Twelve independent rounds of mutagenesis were conducted. Approximately 11,000 mutagenized colonies were screened using fluorescence microscopy in the first eight rounds, and six mutants of interest were recovered. The final four rounds were initially screened in parallel via Fluorescent Activated Cell Sorting (FACS), as described below, and three mutants of interest were isolated (each mutant was selected from an independent culture). Mutants of interest were assigned a unique identifier during screening and identification (Supplementary Figure S1), but throughout the text are referenced by the associated mutant allele, *i.e., sir1-P23S* or *sir2-G436D*.

FACS single-sort

Following EMS mutagenesis, independent mutagenized cultures were grown in liquid medium prior to parallel FACS sorting. Specifically, after the final resuspension in 500 uL YPD ($\sim 2 \times 10^8$ cells), for each independent culture, 50 ml of YPD were inoculated with the mutagenized cells and grown to saturation overnight. The following day, saturated cultures were back diluted to 0.1 OD in YPD and grown to log phase (∼0.6–1.0 OD). Two milliliters of each log-phase culture was harvested, washed, and resuspended in 2 ml 1X sterile PBS. Samples were strained through a 5 μm sterile mesh cap into a 5 ml polypropylene tube (Falcon), and kept on ice until sorting. SIR^+ and *sir4Δ* control strains (JRY12860 and JRY12862) were used to determine fluorescence threshold levels, as all SIR^+ cells were nonfluorescent, and all *sir4Δ* cells were fluorescent. One large gate for fluorescent cells (only GFP^+, only RFP^+, and GFP^+ and RFP^+) was created, and fluorescent cells (approximately 10,000 per culture) were sorted, grown at 30°C overnight, and then plated for screening. Plates were incubated at 30°C until colonies formed and were large enough for screening (2–4 days). Only a single mutant of interest was followed from each independent mutagenized culture.

FACS double-sort

Double FACS sorting was performed for one round of mutagenesis. Strain JRY11906 was mutagenized. The first part of the double-sort strategy was identical to the single-sort strategy. Sorted fluorescent cells were then grown at 30°C in liquid culture overnight. Fresh YPD was inoculated with the daughters of the sorted cells to a density of 0.1 OD, and maintained near log-phase growth through continuous back dilution for 2 days, providing ample time for some fluorescent cells to switch into a silenced state. After these 2 days of growth, samples were prepared for sorting as above, but this time a gate for GFP^- and RFP^- cells was created, and these sorted cells were grown at 30°C in YPD overnight and prepared for colony screening as indicated above. Again, a single mutant of interest was followed per independent mutagenized culture.

Colony imaging

Cells were plated at a low density (20–35 cells/plate) on solid medium as indicated in individual figures. Single cells were then grown into colonies for 3–5 days at 30°C and imaged using a Leica M205 FA fluorescence stereomicroscope and a Leica DFC3000 G microscope camera equipped with LAS X software (Leica). For all

colony images within a given experiment, all conditions (growth, media, magnification, and exposure) were identical.

Flow cytometry

Cells were inoculated into 150 uL of CSM in 96-well plates (Corning). Three biological replicates per strain were grown overnight. Saturated cultures were back diluted to ~0.1 OD in fresh CSM, and continuously back diluted to maintain log-phase growth for 24 h; this growth period allowed the distribution of cells with silenced or nonsilenced *HML* and *HMR* to reach equilibrium. After 24 h of log-phase growth, cells were harvested by centrifugation, resuspended in 100 µL of 4% paraformaldehyde, and incubated at room temperature for 15 min. Samples were pelleted and the fixed cells were resuspended in 100–150 uL of a 1X PBS solution. These fixed samples were stored at 4°C and analyzed by flow cytometry within 5 h of fixation. Flow cytometry was performed using a BD LSRFortessa (BD Biosciences) with a FITC filter (for GFP) and a PE-TexasRed filter (for RFP), and at least 10,000 cells were analyzed per sample. Flow cytometry data were analyzed and visualized using FlowJo (BD Biosciences). All flow cytometry data were gated identically, omitting aggregates and cellular debris from analysis.

Immunoblotting

Protein isolation, immunoblotting, and quantification were carried out as previously described (Brothers and Rine 2019). The membranes were blocked in Odyssey Blocking Buffer (LI-COR Biosciences), and the following primary antibodies and dilutions were used for detection: mouse anti-V5 (Invitrogen R960-25, 1:5,000) and rabbit anti-Hxk2 (Rockland #100-4159, 1:10,000). The secondary antibodies used were goat anti-rabbit (Li-Cor #C60531-05 1:20,000) and goat anti-mouse (Li-Cor #C81106-03 1:20,000). The immunoblot was imaged using a Li-Cor infrared fluorescent scanner.

Patch mating assay

Strains to be assayed were patched onto solid YPD and grown at 30°C. After 1 day, these YPD plates were replica plated onto a mating-type tester lawn with complementary auxotrophic markers (*MATa* JRY2726, and *MATα* JRY2728, plated on YPD), and grown at 30°C for 1 day. Lawns were then replicated onto minimal YM medium, grown at 30°C for 2 days, and imaged.

α-factor confrontation assay

This assay was carried out as previously described (Pillus and Rine 1989). Single, unbudded cells were micromanipulated approximately ½ field of view at 200X magnification away from the streak of *MATα* cells which served as a source of α-factor. The plates were incubated at 30°C for approximately 3 h and the morphology of single cells was observed.

Live-cell imaging

Strains JRY12861, JRY12564, and JRY12901 were grown as described above for flow cytometry, but in 5 ml cultures of CSM. After 24 h of log-phase growth, a 500 µL aliquot of cell suspension at approximately 0.6–1.0 OD was harvested and resuspended in 500 uL sterile water. This cellular suspension was then sonicated for 5 s at 20% amplitude (Branson Ultrasonics Digital Sonifier 100-132-888 R with Sonicator Tip 101-135-066 R) to disrupt aggregates. A 5 µL aliquot of sonicated cells was spotted onto a CSM 2% agar pad. Once dry, the agar pads were inverted onto a 35 mm glass-bottom dish (Thermo Scientific) and imaged using a Zeiss Z1 inverted fluorescence microscope with a Prime 95B sCMOS camera (Teledyne Photometrics), Plan-Apochromat 63x/1.40 oil immersion objective (Zeiss) filters, MS-2000 XYZ automated stage (Applied Scientific Instrumentation), and Micro-Manager imaging software (Open Imaging). Samples were incubated at 30°C and imaged every 10 or 15 min for a total of 10 h in bright-field, GFP, and RFP. Time-lapse movies were prepared and analyzed using FIJI software (Schindelin *et al.* 2012).

Single-cell segmentation and fluorescence quantification

Bright-field microscopy images from live-cell imaging were segmented using the online tool Yeast Spotter (Lu *et al.* 2019) or manually for individual cells over long time courses, such as those shown in Figure 3, D and E. Individual cells were parsed and labeled using the "analyze particles" tool in FIJI, and measurements taken, including area and GFP mean fluorescence intensity.

Individual cells were assigned a silencing state of *hmrα2Δ::GFP* ("*HMR* off," "*HMR* intermediate," "*HMR* on"), using threshold values determined from the *sir1Δ* (JRY12861) single-cell analysis data. The *sir1Δ* cell data were split into two populations ("*sir1Δ* off" and "*sir1Δ* on"), with each population assumed to be normally distributed, and the threshold values designated to include 90% of the respective *sir1* population. The "*HMR* off" to "*HMR* intermediate" boundary was defined as the 90th percentile rank GFP fluorescence intensity value for the "*sir1Δ* off" population (798 GFP mean fluorescence intensity). The "*HMR* intermediate" to "*HMR* on" boundary was defined as the 5th percentile rank GFP fluorescence intensity value for the "*sir1Δ* on" population (1103 GFP mean fluorescence intensity). For Supplementary Figure S4, this approach to quantitatively establish thresholds did not yield thresholds that could accurately demarcate the local minimum between the *sir1Δ* "*HML* on" and "*HML* off" populations. Therefore, the thresholds for Supplementary Figure S4 were determined qualitatively from the *sir1Δ* fluorescence analysis, and subsequently applied to *sir2-G436D*.

Pedigree analysis for measuring heritability

Time-lapse microscopy movies (described above) were analyzed to measure the heritability of a fluorescence state. For each pedigree analyzed, a single cell (mother) and three resulting progeny [daughter 1, daughter 2, grand-daughter (daughter of daughter 1)] were manually segmented and the fluorescence state was measured using FIJI software. At each time point ($t = 0$ min, $t = 90$ min, $t = 180$ min), all cells were measured and assigned a fluorescence state, using the threshold values established above. If all progeny at all time points displayed the same expression state as the mother cell had at $t = 0$ min, the pedigree was labeled "heritable," reflecting the heritability of that expression state. If any of the cells in the pedigree switched state designations, the pedigree was labeled as a "switch," reflecting the absence of heritability of that expression state in that pedigree.

rDNA recombination assay

To measure rDNA recombination in *RDN37::yEGFP* strains, cells were grown overnight, back diluted, and plated on YPD at a concentration of 30 cells/plate for sector analysis, or 500 cells/plate for half-sector quantification. To quantify half-sectors, parallel lines were drawn along the plate to demarcate regions of interest, and the viewer manually scanned these regions of interest with a Leica M205 FA fluorescence stereomicroscope and manually counted colonies that exhibited GFP+ signal and either had half-sectors or not.

Results

Identification of metastable mutants

To isolate mutants that displayed metastable silencing defects at *HML* and *HMR*, we utilized an assay that reveals the expression state of these two loci individually. The FLAME assay utilizes fluorescent reporters integrated at *HML* and *HMR*, termed *hmlα2Δ::RFP* and *hmrα2Δ::GFP*, respectively (Saxton and Rine 2019, Figure 1A). In wild-type cells, these loci are stably silenced by the SIR complex (Rine and Herskowitz 1987). Thus, when SIR complex members Sir2, Sir3, or Sir4 are absent, these loci are fully expressed. In the FLAME assay, loss of silencing results in expression of the fluorescence reporters, which can be evaluated at either the single-cell or colony level. The colony phenotype offers additional historical information about the expression state of *HML* and *HMR*. Due to the pattern of cell divisions, ancestors are proximal to their descendants, forming sectors of related cells that radiate to the periphery of the colony. In *sir2*, *sir3*, or *sir4* mutants, colonies are uniformly fluorescent, whereas in a *sir1Δ* mutant, a sectored fluorescence pattern is observed; this sectoring indicates heritable phenotypic variation within a genetically identical population (Figure 1B). By screening colonies arising from the mutagenized *SIR*$^{+}$ reporter strain, we identified six mutants with metastable silencing of *HML* and *HMR* (Supplementary Figure S1A).

As a complement to direct screening of colonies, we adapted fluorescence-activated cell sorting (FACS) to detect and sort fluorescent cells within a mutagenized population. These sorted cells were then interrogated for clonal heritability of expression states at the colony level (see Materials and Methods). Using a double-FACS sorting strategy, three additional mutants of interest were found (Supplementary Figure S1A).

Genetic analysis identified eight unique *sir1* alleles

The metastable phenotype was recessive in all nine mutants of interest, based on the fluorescence of diploids heterozygous for the new mutations (Figure 1C and Supplementary Figure S1B). To

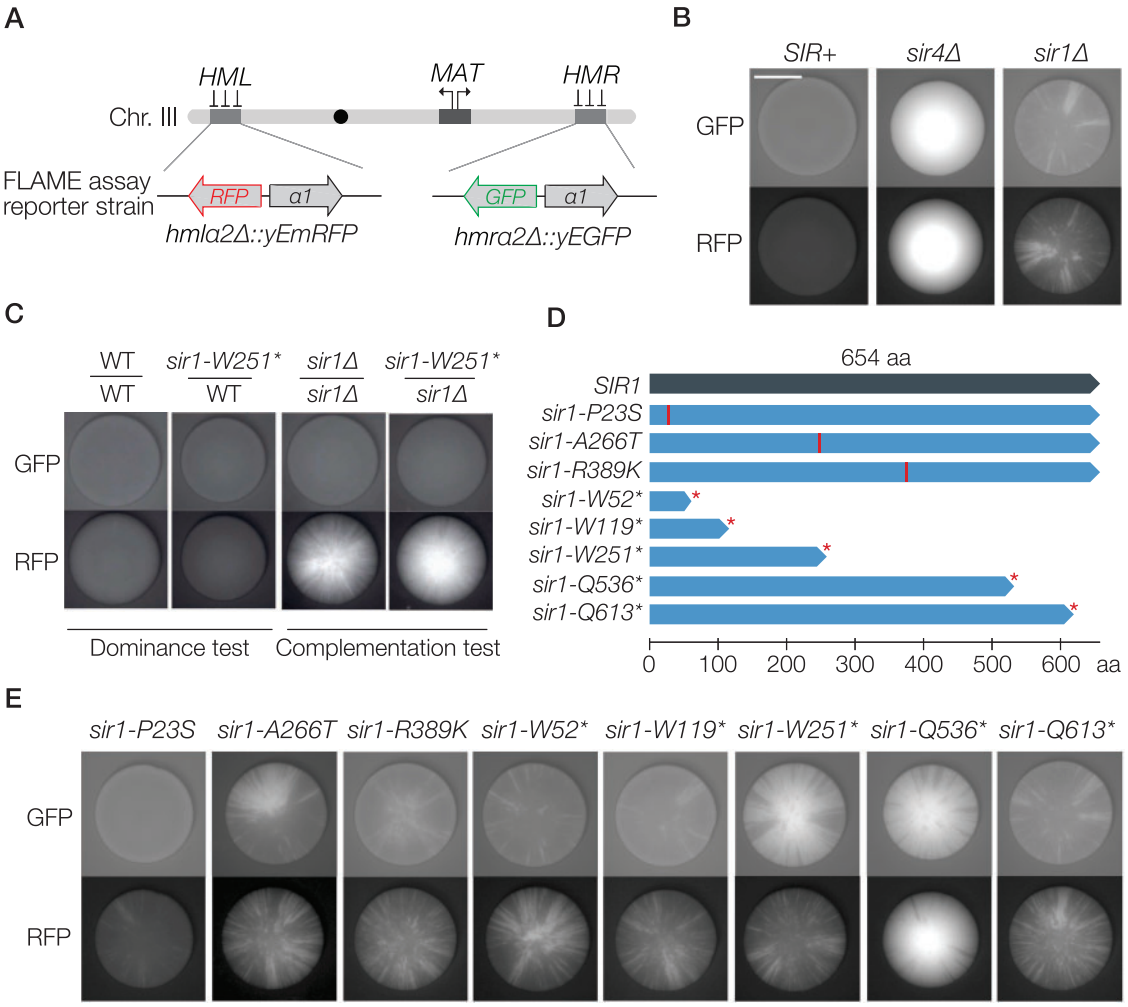

Figure 1 A screen for metastable silencing mutants revealed eight unique alleles of *sir1*. (A) Schematic of the FLAME reporter strain (JRY12860) used in this study: fluorescent reporters *yEGFP* and *yEmRFP* replaced *α2* at *HMRα* and *HMLα*, respectively. (B) Colony phenotypes of control strains (JRY12860–JRY12862) in both the GFP and RFP channel. Colonies were grown on YPD and imaged at identical exposures (Scale bar, 4 mm). (C) Representative colony images of diploid strains for the dominance and complementation tests. For dominance testing, a *MATa* wild-type FLAME strain was mated with *MATα* mutant strain (JRY11955 and JRY11915); for complementation testing, a *MATa sir1Δ* strain was mated with a *MATα* mutant strain (JRY11957 and JRY11950). (D) A schematic of the *sir1* alleles identified. The *SIR1* gene encodes a 654 amino acid protein (top bar in dark blue). Mutant alleles contained either a missense mutation or a nonsense mutation. Premature stop codons are indicated with an asterisk, *i.e.*, *sir1-W52**. (E) Colony images of the engineered single point mutation *sir1* alleles, imaged on YPD in both the GFP and RFP channel. Differences in fluorescence profiles between colonies mostly reflect the high degree of variability between colonies of a given genotype, rather than differences between genotypes.

test if the metastable phenotype was due to a single mutation, seven of the diploids from the dominance test were sporulated and the phenotype evaluated among the tetrad segregants. The characteristic 2:2 segregation of mutant to wild-type phenotypes was observed for at least ten tetrads from each of the mutants tested, strongly suggesting that a mutation in a single gene caused the metastable phenotype.

A complementation test was used to determine whether these mutants revealed new genes capable of metastable phenotypes or were new alleles of *SIR1*. In this test, *MATα* mutants were mated to an isogenic *MATa sir1Δ* strain. All seven mutants tested failed to complement a *sir1Δ* mutation (Figure 1C and Supplementary Figure S1C). Interestingly, in diploids, the silencing phenotype was less severe than in haploids, and far more evident at *HML*. This discrepancy likely reflects previous findings that silencing is stronger in diploids than in haploids (Dodson and Rine 2015), and that haploid *sir1Δ* cells are more frequently silenced at *HMR* than at *HML* (Saxton and Rine 2019).

The *sir1* alleles of each mutant strain were sequenced, revealing mutations within the coding region of *SIR1* (Figure 1D). Two independent rounds of mutagenesis produced identical nonsense mutations, resulting in identical *sir1-W251** alleles. As expected from EMS mutagenesis, all of the *sir1* alleles contained a single point mutation resulting from GC to AT transitions, with five of the eight unique point mutations resulting in a nonsense mutation (Supplementary Figure S1D). These point mutations were engineered into the parent strain using molecular cloning techniques, where they recapitulated the phenotypes observed in the original mutants, showing that the *sir1* alleles were necessary and sufficient to produce the metastable phenotype observed (Figure 1E).

A metastable phenotype from a mutation in *SIR2*

Having identified eight independent and unique *SIR1* alleles, we revised the screening strategy to reduce the likelihood of finding more *sir1* mutants. We reasoned that if two *SIR1* alleles were present in our haploid reporter strain, the probability of random mutagenesis disrupting both in the same cell would be reduced. Therefore, an additional copy of *SIR1* was maintained on a plasmid in the parental strain of the screen (JRY12860 containing pJR909). After mutagenesis, a single-FACS enrichment step was employed (see Materials and Methods). With this additional extrachromosomal copy of *SIR1*, very few mutants with a metastable phenotype were produced. After mutagenizing and sorting 12 independent cultures with FACS, no further *sir1* alleles were found. One colony of interest was identified, which exhibited a mild but noticeable silencing defect (Figure 2A). The phenotype was unlike any other observed during both iterations of mutagenesis and unique from all other mutant phenotypes studied using the FLAME assay. In this mutant, the entire colony exhibited expression of *HML* and *HMR*, but the strength of expression was less than that observed in *sir2Δ*. Moreover, close examination of the colony revealed streaks of greater or lesser fluorescence intensity, suggesting the possibility of heritable intermediate defects in silencing, a phenotype not previously described. The mutant phenotype was recessive, complemented a *sir1Δ* mutation, and produced a 2 wild-type: 2 mutant segregation pattern after diploid sporulation and tetrad analysis (Supplementary Figure S2).

To identify the causative gene resulting in the mutant phenotype, we first assayed the ability of *SIR2, SIR3*, or *SIR4* to rescue the silencing defect. Transformation of a *SIR2* plasmid into the parent strain restored wild-type silencing, whereas *SIR3* and *SIR4* plasmids had no effect on the silencing phenotype. Sir2 is a highly conserved histone deacetylase and is the sole catalytic component of the SIR complex (Imai *et al.* 2000; Landry *et al.* 2000). Sequencing of *SIR2* from the mutant strain revealed a single point mutation at residue 436, changing the encoded amino acid from a glycine to an aspartic acid (*sir2-G436D*). Using molecular cloning techniques, the *sir2-G436D* point mutation was introduced into the parental strain (JRY12564); this mutant recapitulated the intermediate silencing phenotype (Figure 2A). Thus, the missense *sir2-G436D* allele was sufficient to produce the intermediate silencing defect. Colony imaging at longer exposures highlighted the unique fluorescence pattern of this mutant, with streaks of brighter fluorescence superimposed on a low-fluorescence colony (Figure 2B). Interestingly, these streaks of brighter fluorescence overlapped in the RFP and GFP channels, suggesting that *hmlα2Δ::RFP* and *hmrα2Δ::GFP* were coordinately impacted by *sir2-G436D*. The similarity between RFP and GFP channels was not caused by bleedthrough, as streaks were still visualized when only one of the two fluorophores was present (Supplementary Figure S3). Importantly, this concordance between RFP and GFP in *sir2-G436D* contrasted with the colony phenotype of *sir1Δ*, in which *hmlα2Δ::RFP* and *hmrα2Δ::GFP* are silenced or expressed independently of each other (Figure 2A, Xu *et al.* 2006).

A unique silencing defect in *sir2-G436D*

To further characterize this mutant phenotype, flow cytometry was used to quantify the *hmlα2Δ::RFP* and *hmrα2Δ::GFP* fluorescence intensities in log-phase cells. The SIR^+ reporter strain existed as a homogenous population lacking both GFP and RFP fluorescence, whereas the *sir2Δ* strain strongly expressed both GFP and RFP (Figure 2C). Using the SIR^+ and *sir2Δ* control strains, gates were established to create four quadrants representative of the four possible FLAME expression states. As expected, *sir1Δ* cells existed in all four quadrants and therefore exhibited all possible combinations of expression states for *HML* and *HMR*. The *sir2-G436D* mutant strain exhibited a distinct pattern of expression, with a broad spread in fluorescence intensities for *hmrα2Δ::GFP* and *hmlα2Δ::RFP*. The distribution of fluorescence intensities appeared bimodal for *hmrα2Δ::GFP*, and distinctly less so for *hmlα2Δ::RFP*, which was more uniformly expressed. Interestingly, GFP^+ cells and RFP^+ cells appeared less fluorescent in *sir2-G436D* than in *sir1Δ* or *sir2Δ*. Therefore, flow cytometry indicated that *sir2-G436D* cells exhibited either a fully silenced state or intermediate silenced state at both *hmrα2Δ::GFP* and *hmlα2Δ::RFP*.

To evaluate this intermediate silencing phenotype further, the *sir2-G436D* allele was introduced into a strain with wild-type *HML* and *HMR*. Using these strains, silencing of *HML* and *HMR* was measured by a patch mating assay and a single-cell α-factor confrontation assay. In both assays, expression of *HML* or *HMR* causes cells to behave as pseudo *a*/α diploids that don't mate or respond to α factor. In the patch mating test, *sir2-G436D* silenced *HML* and *HMR* inefficiently relative to wild type (Figure 2D). An α-factor confrontation assay (Pillus and Rine 1989) revealed that approximately 7% of *MATa sir2-G436D* cells were able to sufficiently silence *HML* and thus avoid the α-factor resistance of pseudo *a*/α diploids (Figure 2E). Compared to *sir1*, which by α-factor confrontation was previously shown to effectively repress *HML* in 20% of cells, *sir2-G436D* showed a more pronounced silencing defect. Thus, as confirmed by three independent assays, the *sir2-G436D* mutation resulted in partially defective silencing.

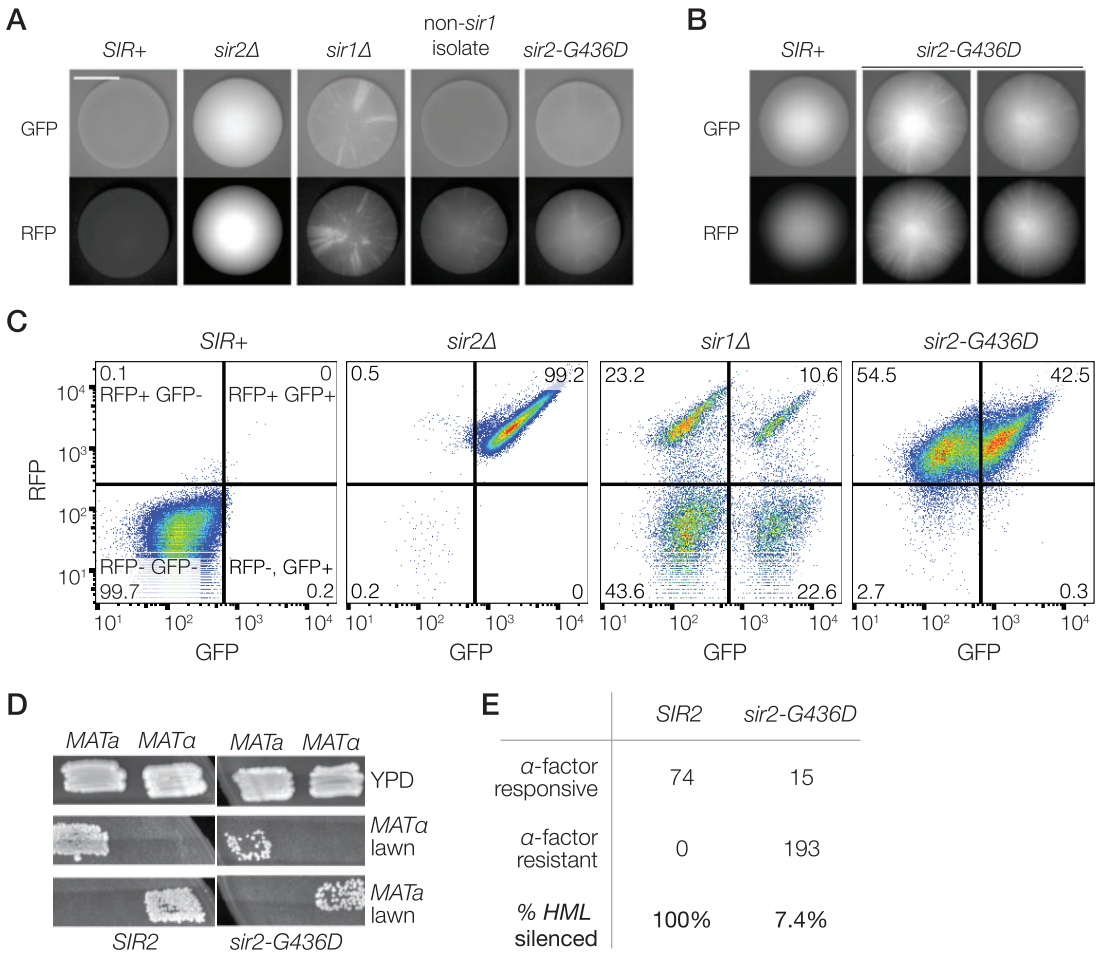

Figure 2 Characterization of mutant *sir2-G436D*. (A) Representative colony images of FLAME control strains, the mutant of interest, and *sir2-G436D* in both the GFP and RFP channel (JRY12860, JRY12259, JRY12861, JRY12466, and JRY12564), grown on YPD. (B) Colony images of FLAME strain SIR^{+} colonies and two biological replicates of the engineered single point mutation strain (JRY12860 and JRY12564). Colonies were grown on CSM and imaged at approximately 10-fold longer exposure than (A) (Scale bar, 4 mm). (C) Flow cytometry plots of the fluorescence profiles for both *hmlα2Δ::RFP* (PE-Texas Red) and *hmrα2Δ::GFP* (FITC). Cells were grown in CSM liquid media for 24 h, fixed, and analyzed. Quadrants were established using *SIR+* and *sir2Δ* strains (JRY12860 and JRY12466), and the resulting percentage of the population per quadrant was labeled in the corresponding corner. *sir1Δ* cells (JRY12861) exhibited distinct populations in all four quadrants, while *sir2-G436D* (JRY12564) cells exhibited fully silenced states and intermediate silenced states. (D) Patch mating assays of *SIR2* and *sir2-G436D* in *MATa* (JRY4012 and JRY12667) and *MATα* (JRY4013 and JRY12669) cells. The extent of growth on the YM minimal media reflected the strength of silencing. A complete loss of silencing, such as that seen in *sir2Δ*, would yield no mating and therefore no growth. (E) Results of the α-factor confrontation assay (JRY4012 and JRY12667). *HML* silencing was calculated by dividing the number of α-factor responsive cells by the total number of cells assayed. A complete loss of silencing, such as that seen in *sir2Δ*, would cause all cells to be α-factor resistant.

sir2-G436D produced intermediate, heritable expression

To monitor the different silencing states of *sir1Δ* and *sir2-G436D* over time, we first tested whether these states were evident by live-cell microscopy. To simplify the analysis by microscopy, we first focused on the expression states of *hmrα2Δ::GFP*. As previously established by RNA FISH (Dodson and Rine 2015), *sir1Δ* cells exhibited either full silencing or full expression of *HMR* (Figure 3A). In partial contrast, *sir2-G436D* cells exhibited full silencing or partial silencing of *HMR* (Figure 3A). To quantify fluorescence levels, cell segmentation and quantification were performed. Using bright-field images, individual cells were segmented with Yeast Spotter (Lu *et al.* 2019). Once segmented, single-cell data were extracted and displayed as a histogram (Figure 3, B and C). As anticipated, cell size was approximately normally distributed, with no meaningful difference between the genotypes (Figure 3B); however, the GFP fluorescence profiles per genotype were distinct. *sir1Δ* cells were either fully silenced or fully expressed, similar to the flow cytometry data, whereas *sir2-G436D* cells were either fully silenced or partially silenced (Figure 3C). Using fluorescence intensities of *sir1Δ* cells, threshold values were established to demarcate three fluorescence states: "*HMR* off," "*HMR* intermediate," and "*HMR* on." Using these thresholds, approximately 40% of the *sir2-G436D* cells measured exhibited intermediate fluorescence ("*HMR* intermediate"), while only 4% of *sir1Δ* cells displayed intermediate expression.

For a transcriptional state to be classified as epigenetic, it must be heritable through cell divisions. Therefore, we assessed the ability of the *sir1Δ* and *sir2-G436D* mutants to reliably transmit the observed silencing states over multiple generations. Time-lapse movies of dividing cells qualitatively suggested that the observed states were heritable (Supplementary Movies 1 and 2). To quantitatively assess this heritability, we monitored the fluorescence of individual mother cells over the course of four

division events, or approximately 6 h. In both *sir1Δ* and *sir2-G436D*, the fluorescence states of individual cells could be maintained over this entire period or switch to a different state (Figure 3, D and E). In addition, the frequency at which a *sir2-G436D* mother-daughter pair exhibited the same fluorescence state was significantly higher than the frequency at which two randomly chosen cells exhibited the same state (Figure 3F).

To calculate approximate switching rates, unbudded cells and the resulting progeny of two generations were manually tracked, and each cell assigned an *HMR* expression state according to the threshold values in Figure 3C. A pedigree was designated as "heritable" if all cells within the pedigree exhibited the same expression state of *HMR* at all three time points (Figure 3G). In contrast, the pedigree was designated as a "switch" if any of the cells within the pedigree switched to a different *HMR* expression state. Two generations were analyzed to increase our confidence that the *HMR* expression states were heritable and did not simply reflect variation in fluorescent properties of individual cells. Using this method, 250 pedigrees per genotype were analyzed (Figure 3H).

Recent studies using microscopy and flow cytometry show that approximately 10% of *sir1Δ* cell divisions give rise to a switch in *HMR* expression state (Saxton and Rine 2019). Consistent with this finding, approximately 10% of *sir1Δ* pedigrees analyzed resulted in a switch in *HMR* silencing, while the other 90% of pedigrees displayed heritability (Figure 3H). The occurrence of switching in *sir2-G436D* was higher than in *sir1Δ*. However, a majority of pedigrees, approximately 62%, displayed heritability of the *HMR* expression state. Though the majority of these heritable pedigrees displayed "*HMR* off" silencing, 28% of the *sir2-G436D* pedigrees analyzed showed stable transmission of the "*HMR* intermediate" state. This live-cell imaging analysis further supported that *sir2-G436D* exhibited an intermediate silenced state and showed that this state was inherited through cellular division.

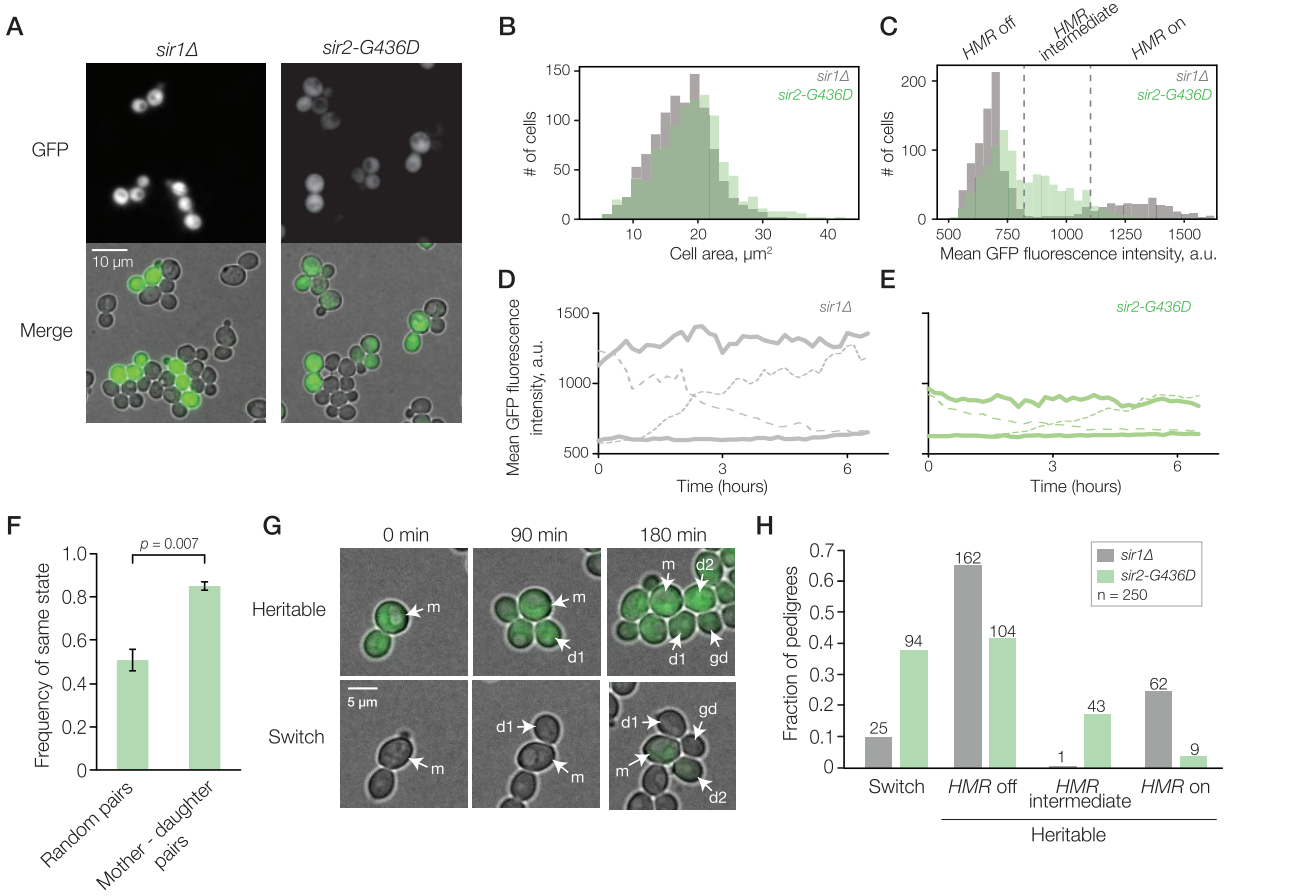

Figure 3 Live-cell imaging revealed the intermediate and heritable *sir2-G436D* expression state. (A) GFP and merged (bright-field and GFP) fluorescence microscopy images of *sir1Δ* and *sir2-G436D* cells (JRY12861 and JRY12564), imaged with identical exposures. (B) Distribution of the cell size for both *sir1Δ* and *sir2-G436D*, with number of cells on the y-axis and cell area in μm^2 on the x-axis. (C) Distribution of the GFP mean fluorescence intensity (arbitrary units, a.u.) per cell for both *sir1Δ* and *sir2-G436D*. Dashed lines demarcate the boundaries of the three fluorescence states: *HMR* off, *HMR* intermediate, and *HMR* on. Details on how thresholds were assigned are in Materials and Methods. (D) GFP mean fluorescence intensity for individual *sir1Δ* cells over 6.5 h. Twelve individual cells were monitored, and 4 representative fluorescence trajectories are displayed. Each solid line represents a single cell that maintained a similar fluorescence level over the timecourse, whereas each dashed line represents a single cell that experienced a change in fluorescence. (E) Same as (D), but for 4 individual *sir2-G436D* cells. (F) Frequency at which either mother–daughter pairs or random pairs of cells exhibited the same expression state, as determined by threshold values in (C). Five different fields-of-view were analyzed ($n > 50$ random pairs and $n > 50$ mother–daughter pairs per field-of-view). Data are means ± SD. A two-tailed *t*-test was used for statistical analysis. (G) An example of the pattern of divisions and pedigrees designated as "heritable" versus a "switch" in *sir2-G436D* cells. A single mother cell (m, t = 0 min) budded twice, producing daughter 1 (d1, t = 90 min) and daughter 2 (d2, t = 180 min). Budding of daughter 1 gave rise to a grand-daughter (gd, t = 180 min) cell. In the "heritable" example, all cells at all time points displayed a fluorescence level falling within the "*HMR* intermediate" range; in the "switch" example, a loss of silencing occurred during the second division, giving rise to cells with fluorescence classified as "*HMR* intermediate." (H) Bar chart showing the fraction of pedigrees designated as a "switch" or "heritable." Two hundred and fifty pedigrees were observed per genotype, with the number of pedigrees per category above each bar.

To further test if *sir2-G436D* yields heritable states of intermediate silencing, we also analyzed expression of *hmlα2Δ::RFP* by microscopy. Consistent with flow cytometry, *sir1Δ* exhibited a mix of cells that were either fully silenced or fully expressed at *HML*, and *sir2-G436D* cells were mostly in the intermediate silenced state, though some were fully silenced (Supplementary Figure S4, A–C). The same single-cell analyses that were performed on *HMR* in Figure 3 were also applied to *HML*, and strongly suggested that the different expression states of *HML* were heritable in both *sir1Δ* and *sir2-G436D* (Supplementary Figure S4, D–F, Supplementary Movies 1 and 2). In addition, an analysis of concordance between the expression states of *HML* and *HMR* suggested that the states at each locus were at least partly independent (Supplementary Figure S4G). Therefore, a heritable intermediate silenced state was observed at *HML* in some *sir2-G436D* cells, similar to *HMR*.

sir2-G436D silencing defects were partially due to reduced levels of Sir2

Based on the crystal structure of the Sir2 protein (Hall and Ellenberger, unpublished results; Hsu *et al.* 2013), codon 436 falls within the highly conserved C-terminal catalytic domain. However, residue 436 is distinct from the site of catalysis and is in close proximity to the zinc ion within the zinc-finger domain (Figure 4A). A previous study found that disruption of the zinc-finger domain by mutation of the coordinating cysteine residues results in full silencing loss (Sherman *et al.* 1999). Strikingly, the aspartic acid introduced by the *sir2-G436D* mutation is predicted to encroach on the zinc-coordinating site, which may disrupt the protein stability and silencing capacity of Sir2-G436D (Figure 4A).

To test whether this mutation affected the stability of Sir2, the wild-type and mutant Sir2 proteins were tagged with the V5 epitope and protein levels were evaluated by immuno-blot. Mutant Sir2-G436D levels were roughly 40% of the wild-type Sir2 levels (Figure 4B, Supplementary Figure S5). If this reduced expression was responsible for the observed silencing defects, we would expect that higher expression of *sir2-G436D* would ameliorate these defects. Indeed, expression of *sir2-G436D* from a high copy number plasmid reduced the amount of variegation in the *sir2-G436D* mutant strain, as compared with a vector-only control (Figure 4C, Supplementary Figure S6A). These data suggested that the *sir2-G436D* silencing defect was partially due to reduced levels of Sir2-G436D. Surprisingly, the effects of this *sir2-G436D* plasmid were not observed by flow cytometry (Figure 4, D and E, Supplementary Figure S6B). This discrepancy provided an early indication that the

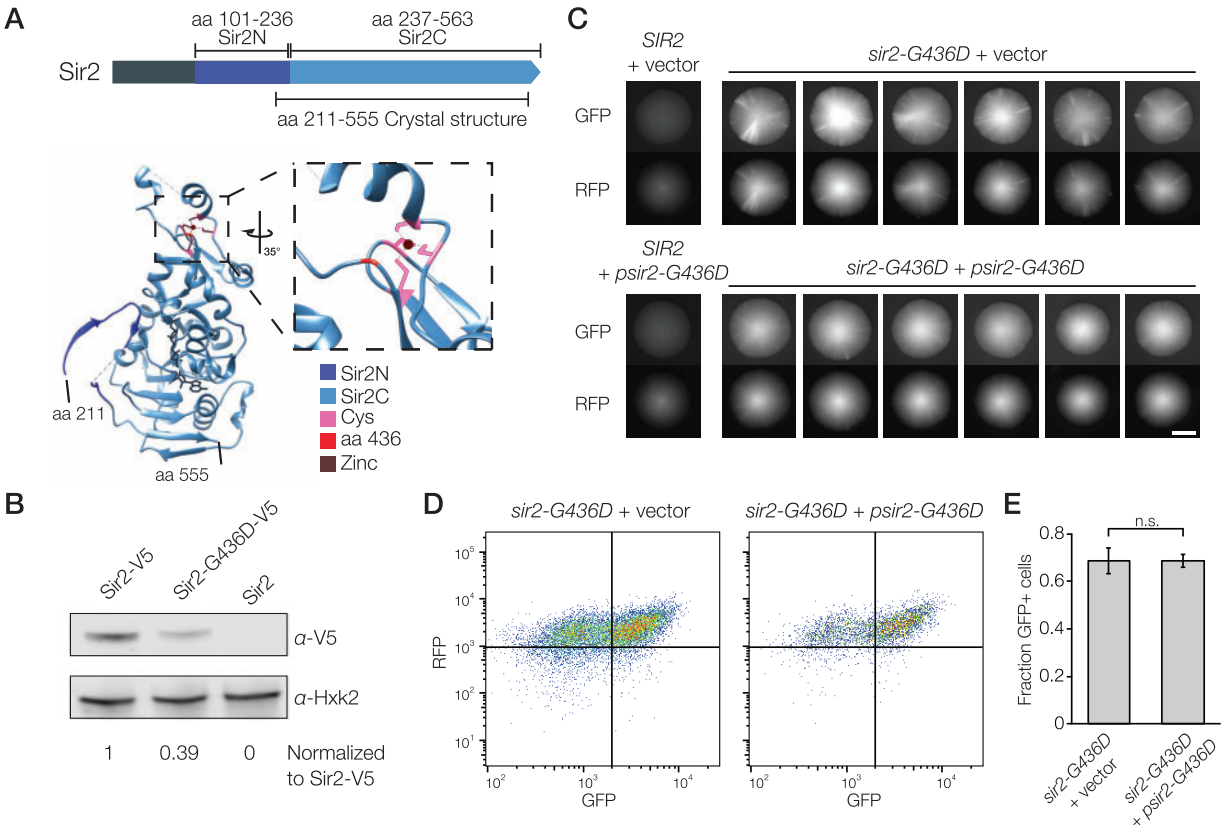

Figure 4 Sir2-G436D levels were partially responsible for variegated silencing. (A) A schematic of the Sir2 protein and its crystal structure (Hall and Ellenberger, unpublished results; Hsu *et al.* 2013). The N-terminal helical domain (dark blue) and C-terminal catalytic domain (light blue) are indicated. The crystal structure spans from amino acid 211-555 and contains a zinc ion (brown), zinc-coordinating cysteines (pink), and the site of the Sir2-G436D point mutation (red). The inset shows the zinc-coordinating site in Sir2. (B) Immunoblot to detect Sir2-V5, Sir2-G436D-V5, and an internal loading control Hxk2 (JRY12589, JRY12590). Protein levels were quantified, normalized to the loading control, and compared to wild-type Sir2-V5 levels. A biological replicate was performed and is presented in Supplementary Figure S5. (C) Representative colony images of *SIR2* (JRY12860) or *sir2-G436D* (JRY12564) plus a 2-micron plasmid vector (pRS426) or a 2-micron plasmid containing *sir2-G436D* (pJR3525). Six colonies are shown for each *sir2-G436D* strain. Colonies were grown on CSM -Ura to select for plasmids. Scale bar, 3 mm. (D) Representative flow cytometry profiles of same strains shown in (C). Independent cultures ($n = 3$ per genotype) were grown at log phase for 24 h in CSM -Ura liquid media, fixed, and analyzed. Representative flow cytometry profiles for each strain are shown. Quadrants were established by using the fluorescence profiles of *SIR2* and *sir2Δ* cells (Supplementary Figure S6). (E) Fraction of GFP^+ cells in independent cultures grown in (D). Data are means ± SD ($n = 3$ independent cultures per genotype). A two-tailed *t*-test was used for statistical analysis.

variegation observed in *sir2-G436D* colonies was a relatively small part of the heritability observed at the single-cell level. This idea is explored further in the subsequent section.

rDNA recombination accounted for variegated silencing in *sir2-G436D* colonies

In addition to its role in silencing at *HML*, *HMR*, and telomeres, Sir2 is also part of the RENT complex, which binds to rDNA and suppresses recombination between rDNA repeats (Gottlieb and Esposito 1989; Straight *et al.* 1999; Kobayashi *et al.* 2004). Though this activity stabilizes the rDNA copy number, the copy number can still expand and contract in *SIR2* cells. A previous study found that cells with low rDNA copy numbers exhibit stronger heterochromatic silencing at an artificial telomere and destabilized version of *HMR*, suggesting that the SIR complex competes with the RENT complex for a limiting amount of Sir2 (Michel *et al.* 2005). By extension, this study suggests that different rDNA copy numbers require different amounts of the RENT complex, which changes the amount of Sir2 that is available for heterochromatic silencing. Therefore, heritable differences in rDNA copy number may lead to the heritable differences in silencing efficiency in *sir2-G436D*.

Fob1 is a nucleolar protein that functions to create replication fork barriers in the rDNA, which prevent collisions between DNA polymerase and RNA polymerase I (Kobayashi and Horiuchi 1996; Kobayashi *et al.* 1998). In addition, replication fork barriers generate recombinogenic replication intermediates that drive the expansion and contraction of rDNA repeats. Thus, in the absence of *FOB1*, recombination in the rDNA is greatly reduced. To test if changes in rDNA copy number contributed to changes in silencing states of *HML* and *HMR*, we generated a *sir2-G436D*, *fob1*Δ double mutant. In comparison to *sir2-G436D*, the *sir2-G436D*, *fob1*Δ double mutant exhibited substantially less variegation of *HML* and *HMR* expression at the colony level (Figure 5A, Supplementary Figure S7A). These data suggested that rDNA recombination plays a role in the *sir2-G436D* silencing defect.

Though the variegation at the colony level was strongly reduced in the *sir2-G436D*, *fob1*Δ double mutant, these colonies still exhibited a uniform hazy fluorescence. Therefore, we tested whether *fob1*Δ altered the fluorescence profiles of single cells. Similar to the *sir2-G436D* single mutant, *sir2-G436D*, *fob1*Δ double mutant cells were either fully silenced or silenced to an intermediate level and exhibited switching events between these two states (Figure 5, B–E, Supplementary Movie S3. In addition, the *sir2-G436D*, *fob1*Δ double mutant exhibited fewer cells in the intermediate silenced state (Figure 5, B and C). This may suggest a difference in switching rates between states in *sir2-G436D* and *sir2-G436D*, *fob1*Δ, though a calculation of these switching rates by timelapse microscopy did not reveal significant differences (Figure 5, D and E). Together, these data suggested that the heritability of silencing at the single-cell level was partially independent of rDNA copy number. In this framework, our data indicated that *sir2-G436D* silencing defects reflected an admixture of two phenomena: (1) switching events that occurred with a high frequency at the single-cell level, which manifested as intermediate, hazy fluorescence at the colony level and was not heavily influenced by rDNA copy number, and (2) switching events that were difficult to observe in single cells, but were readily observed at the macroscopic level of a colony, and due to changes in rDNA copy number.

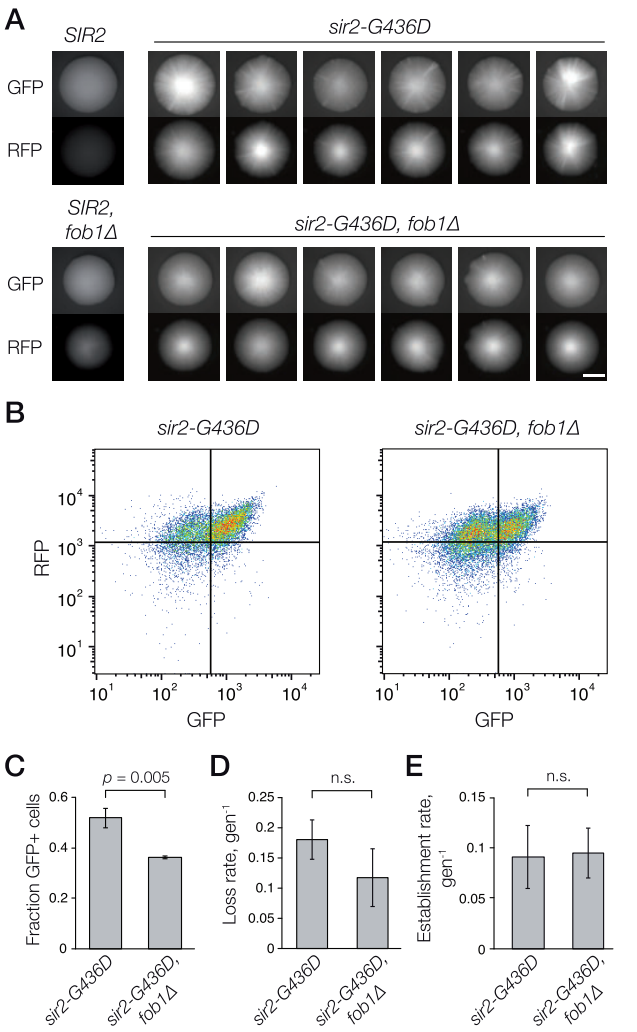

Figure 5 Changes in rDNA copy number were partially responsible for silencing variegation in *sir2-G436D*. (A) Representative colony images of *SIR2* (JRY12860), *SIR2*, *fob1*Δ (JRY12899), *sir2-G436D* (JRY12564), and *sir2-G436D*, *fob1*Δ (JRY12901). Six colonies are shown for each strain with *sir2-G436D*. Colonies were grown on CSM. Scale bar, 3 mm. (B) Flow cytometry profiles of same strains shown in (A). Independent cultures ($n = 3$ per genotype) were grown at log phase for 24 h in CSM liquid media, fixed, and analyzed. A representative flow cytometry flow profile for each strain is shown. (C) Fraction of GFP^+ cells in independent cultures grown in (B). Data are means ± SD ($n = 3$ independent cultures per genotype). A two-tailed *t*-test was used for statistical analysis. (D) The rate of silencing loss per generation, which represented the frequency at which a GFP^- cell switched to GFP^+ per cell division, as calculated by monitoring cell divisions by live-cell microscopy ($n > 500$ cell divisions per genotype). Error bars represent 95% confidence intervals, and statistical analysis was performed by using a Yates chi-square test. (E) The rate of silencing establishment per generation, which represented the frequency at which a GFP^+ cell switched to GFP^- per cell division, as calculated by monitoring cell divisions by live-cell microscopy ($n > 400$ cell divisions per genotype). Error bars represent 95% confidence intervals, and statistical analysis was performed by using a Yates chi-square test.

sir2-G436D affects rDNA recombination rates

Given that rDNA recombination strongly contributed to the variegated silencing observed in *sir2-G436D* colonies, we tested whether *sir2-G436D* influences rates of rDNA recombination *per se*. Previous studies utilize reporter genes that are inserted at a single location in the rDNA and use the rate of reporter gene loss as a proxy for the rate of rDNA recombination (Merker and Klein

2002; Kobayashi *et al.* 2004). To this end, we inserted *GFP* into rDNA and monitored the rate of *GFP* loss in different strain backgrounds. Importantly, these strains did not contain *GFP* at any other genomic location, such as *HML* or *HMR*. To assess the rate of *GFP* loss, we plated and analyzed colonies of each strain. The frequency of GFP$^-$ sectors in an otherwise GFP$^+$ colony provides a qualitative measure of the loss rate. In addition, rare colonies that exhibit half sectors (*i.e.*, one-half of the colony is completely GFP$^-$) reflect colonies in which the first cell division yielded a single loss event; therefore, the frequency of half-sectors reflects the *GFP* loss rate per cell division.

To test the role of *sir2-G436D* in rDNA recombination, we examined *sir2-G436D* alongside other mutations that affect rDNA recombination rates. Consistent with previous studies, *sir2*Δ increased the rate of rDNA recombination, and *fob1*Δ strongly reduced the rate of rDNA recombination (Figure 6, A and B). Surprisingly, *sir2-G436D* increased the rate of rDNA recombination to similar levels as *sir2*Δ, indicating that this mutation abolishes the role of Sir2 in suppressing rDNA recombination. A previous study found that the *fob1*Δ, *sir2*Δ double mutant exhibits a similar rDNA recombination rate as *fob1*Δ, indicating that *fob1*Δ is epistatic to *sir2*Δ (Kobayashi *et al.* 2004). Similarly, we found that *fob1*Δ was epistatic to *sir2-G436D* by this criterion.

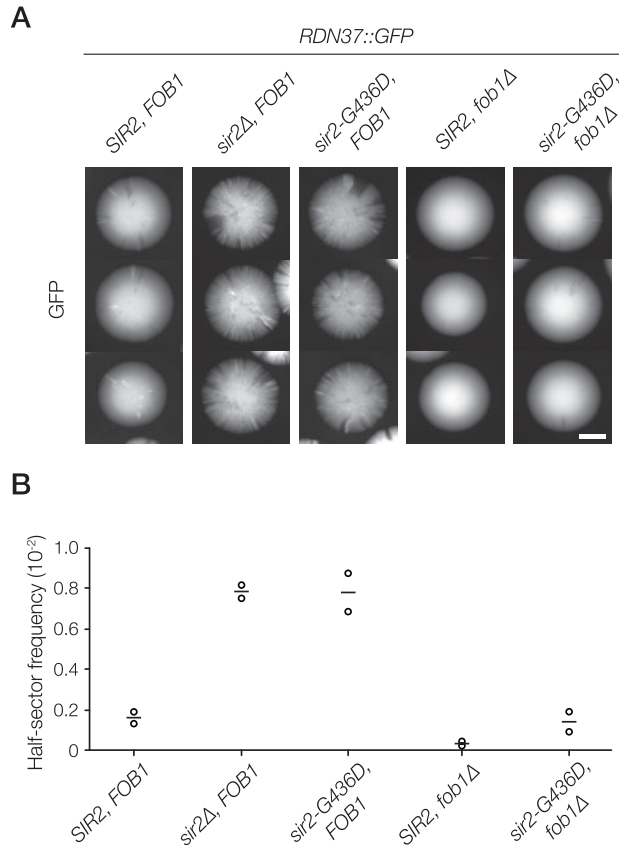

Figure 6 *sir2-G436D* lacks the ability to repress rDNA recombination. (A) Representative colony images of strains containing *RDN37::GFP* (JRY13204-13208), grown on CSM. Three colonies are shown for each genotype. GFP$^-$ sectors represent events in which rDNA recombination yielded a loss of *GFP*, and sectors with stronger GFP signal represent events in which rDNA recombination likely yielded a duplication of *GFP*. Scale bar, 2 mm. (B) Quantification of half-sector frequency for strains containing *RDN37::GFP* (JRY13204-13208), as described in Materials and Methods. Each circle represents the frequency of half-sector colonies in an independent experiment, and lines represent the means of both experiments. At least 7000 GFP$^+$ colonies were analyzed per genotype.

These data strongly suggested that the *sir2-G436D* mutation affected the role of Sir2 at rDNA, in addition to the role of Sir2 at silenced loci.

Discussion

The ability of cells to "remember" a silenced state has historically been uncovered by mutations that generate variegated expression. Despite the value of these mutations, such as *sir1*Δ, previous studies have not systematically screened for variegated silencing phenotypes in *S. cerevisiae*. Here, we performed a metastability screen that uncovered multiple new alleles of *SIR1*, but also identified a novel allele of *SIR2* that exhibited a heritable, intermediate silenced state. Further characterization of *sir2-G436D* revealed that the heritability of this state was not based on rDNA copy number, though changes in rDNA copy number influenced the silencing profile at the colony level. In addition, this mutation affected the role of Sir2 at rDNA.

Sir1 was the main factor preventing metastable silencing of *HML* and *HMR*

Using a forward genetic screen and an assay for metastable silencing defects, we identified nine independent mutant alleles of *sir1*, of which eight were unique. Thus, to a first approximation, the screen had been saturated. It was therefore unlikely that variable penetrance of the *sir1*Δ silencing phenotype was due to a second nonessential gene with overlapping function. Once an additional copy of *SIR1* was introduced for screening purposes, no further *sir1* alleles were found, and very few mutants displayed a metastable phenotype. These results strongly suggested that Sir1 was the most important protein in converting silencing of *HML* and *HMR* from a metastable to fully silenced regime. This idea is consistent with a previous study in which metastable silencing at a telomeric reporter was strengthened by ectopic recruitment of Sir1 (Chien *et al.* 1993).

The unique phenotype of *sir2-G436D*

A novel mutation, *sir2-G436D*, was identified with two striking qualities: (1) The mutation created an intermediate level of silencing, which was heritable through cell divisions as documented by single-cell analysis. (2) At the colony level, this intermediate level of silencing was accompanied by radial streaks of cells with different expression states of the fluorescent reporters. Before discussing the phenotype of this mutant in detail, it is useful to consider the growth dynamics of a yeast colony. Any cell in a colony is a descendant from its more centrally located ancestors. When there is a heritable change in the expression state of a fluorescent reporter gene, that expression state is propagated outward, resulting in a wedge-shaped sector of cells that all exhibit the same state. Thus, a fluorescent sector represents a historical record of a transcriptional switching event that occurred at the apex of the sector, and that was inherited during subsequent colony growth.

The colony-level phenotype of *sir2-G436D* differed from that of *sir1*Δ in multiple ways. First, fluorescent sectors were less fluorescent in *sir2-G436D*, suggesting that the cells in these streaks also had an intermediate level of silencing. Second, the fluorescent sectors were more frequent in *sir2-G436D*, indicating that the switching rate between expression states differed from that seen in *sir1*Δ. Finally, *sir2-G436D* exhibited high concordance between the GFP and RFP channel (Figure 2B), implying that *HML* and *HMR* were coordinately impacted during the majority of the colony growth. This observation strongly suggested that the process

responsible for radial streaks of fluorescence acted in *trans*. In contrast, the expression states of *HML* and *HMR* behave independently of each other in *sir1*Δ (Xu *et al.* 2006, Figure 1B), demonstrating *cis*-transmission of expression states in this context. Together, these data suggested that the variegated expression seen in *sir2-G436D* and *sir1*Δ colonies were driven by fundamentally different mechanisms.

rDNA copy number contributed to variegated expression in *sir2-G436D*

Given that deletion of *SIR2* causes full loss of silencing, it was likely that *sir2-G436D* was a hypomorphic allele. The G436D mutation was predicted to affect the zinc finger domain by generating a large polar side chain that disrupted the zinc finger domain (Figure 4). A previous study found that mutation of the four cysteine residues that coordinate with the zinc ion does not affect Sir2 levels but abolishes the silencing capacity of this protein (Sherman *et al.* 1999). In contrast, Sir2-G436D protein levels were reduced by 40% compared to wild-type Sir2 and exhibited a partial silencing defect. This dichotomy suggested that the Sir2-G436D may have partially disrupted the function of the zinc-coordinating domain and destabilized the mutant protein. Thus, altered levels of Sir2-G436D may be responsible for the silencing defects observed in this mutant. Consistent with this idea, overexpression of *sir2-G436D* from a high copy number plasmid strongly reduced silencing variegation observed at the colony level (Figure 4).

Sir2 is a protein that has multiple functions at different genomic locations. At silenced loci, Sir2 is part of the Sir2/3/4 complex and functions to deacetylate H4K16, which is necessary for silencing (Moazed and Johnson 1996; Imai *et al.* 2000; Landry *et al.* 2000). Separately, Sir2 is part of the RENT complex at rDNA repeats, where it stabilizes rDNA copy number by repressing transcription and regulating cohesin dynamics (Gottlieb and Esposito 1989; Straight *et al.* 1999; Kobayashi and Ganley 2005). Previous studies demonstrate that lower rDNA copy numbers enhance Sir2/3/4-dependent silencing at telomeres, suggesting that the RENT complex and Sir2/3/4 complex compete for a limited amount of Sir2 (Michel *et al.* 2005). We hypothesized that this competition for Sir2 was the underlying mechanism for the variegation observed in *sir2-G436D*. In this model, variation in rDNA copy number would change the amount of rDNA-bound RENT complex, which would then change the amount of Sir2 available for silencing at loci such as *HML* and *HMR*. This model would be consistent with coregulation of *HML* and *HMR* observed at the colony level in *sir2-G436D*, as altered levels of free Sir2 would influence *HML* and *HMR* equally in *trans*.

This model predicted that cells with a reduced ability to change rDNA copy number would exhibit reduced variegation of silencing in *sir2-G436D*. Indeed, removal of *FOB1*, which is necessary for rDNA recombination, strongly reduced the silencing variegation of *HML* and *HMR* in this context. These data strongly suggested that the heritability of expression states observed in *sir2-G436D* was due to rDNA copy number. In light of this finding, we speculated that under normal conditions, Sir2 levels were high enough that Sir2/3/4 and RENT complexes were not in conflict over Sir2. In contrast, *sir2-G436D* reduced Sir2-G436D levels such that it could not simultaneously meet the requirements of both the Sir2/3/4 and RENT complexes.

Though heterochromatic silencing is often framed as an epigenetic mechanism, our data suggested that genetically heritable differences in rDNA copy number is an additional mechanism that can lead to variable yet heritable expression states of heterochromatin. The genetic heritability of different rDNA copy numbers is broadly conserved (Lyckegaard and Clark 1989; Zhang *et al.* 1990; Gibbons *et al.* 2015), and it is interesting to speculate how cells either utilize or mitigate the effects of this variation. In yeast, different rDNA copy numbers are linked to differences in gene silencing, the monitoring of replication initiation, and replicative lifespan (Kaeberlein *et al.* 1999; Michel *et al.* 2005; Ganley *et al.* 2009). Whether these differences provide adaptive benefits or simply reflect the competition of different cellular processes over limiting factors, such as Sir2, will certainly be a motivating question for future studies.

The impact of *sir2-G436D* on rDNA recombination

Previous studies show that Sir2 represses recombination between rDNA repeats (Kobayashi *et al.* 2004). Specifically, *sir2*Δ increases the rate of rDNA recombination in a *FOB1*-dependent manner. We found that *sir2-G436D* increased rDNA recombination rates to the same degree as *sir2*Δ, and that this effect was also dependent on *FOB1*. These data suggested that *sir2-G436D* lacked a central function of Sir2 at rDNA.

The effect of *sir2-G436D* at rDNA was interesting in light of variegated silencing defects observed at the colony level. If variegated silencing at the colony level was the result of fluctuating ratios of Sir2-G436D bound at rDNA versus silenced loci, yet Sir2-G436D cannot suppress rDNA recombination, then Sir2-G436D would be recruited rDNA but exist in an inactive conformation or be catalytically inefficient.

A recent study demonstrated that rDNA copy number influences the transcriptional activation of *SIR2*, providing a feedback mechanism for proper maintenance of rDNA copy number (Iida and Kobayashi 2019). In light of our findings, this feedback mechanism suggests that the *sir2-G436D* mutant may have an interesting array of cause-effect relationships between (1) transcriptional silencing of *HML* and *HMR*, (2) the rate of rDNA recombination, and (3) expression levels of *sir2-G436D*. Though *fob1*Δ is able to simplify this network of factors by substantially reducing rDNA recombination, future studies that focus on complex circuitries may benefit from alleles such as *sir2-G436D*.

The existence of an intermediate silenced state

Single-cell analysis is useful to study heritable expression states in a cell population; this concept has been illustrated by multiple studies that uncovered and characterized the epigenetic states seen in *sir1*Δ (Pillus and Rine 1989; Xu *et al.* 2006). One important aspect of silencing in *sir1*Δ is that silenced cells are silenced to the same degree as SIR^+ cells, and expressed cells are expressed to the same degree as *sir2*Δ cells (Figure 2). In contrast, *sir2-G436D* exhibited a mix of silenced cells and cells that exhibited intermediate expression, as measured by flow cytometry and microscopy. Remarkably, these intermediate states were heritable through multiple cell divisions.

Curiously, overexpression of *sir2-G436D* did not influence the frequency of different expression states seen in *sir2-G436D* by flow cytometry, and *fob1*Δ had relatively small effects on this frequency. This result contrasted with the ability of *sir2-G436D* overexpression to partially reduce, and of *fob1*Δ to strongly reduce, variegation of silencing at the colony level. Together, these results suggested that the majority of switching events at the single-cell level were independent of changes in rDNA copy number and the associated colony-level variegation. In this model, a relatively high switching rate between silencing states of *sir2-G436D* manifested as uniform, intermediate fluorescence at the colony level in *fob1*Δ. Then, the added layer of rDNA copy number

changes in *FOB1* altered heritability of these silencing states in a manner that was relatively small or absent at the single-cell level, but readily observed as radial streaks at the macroscopic level of a colony. Therefore, the intermediate expression state observed in *sir2-G436D* was mostly independent of changes in rDNA copy number and may have derived from a unique behavior of the Sir2-G436D protein at silenced loci.

A recent study found that Sir-based silencing establishment at both *HML* and *HMR* occurs through an intermediate silenced state, rather than an abrupt switch from the fully expressed to fully silenced state (Goodnight and Rine 2020). Furthermore, this intermediate state could be generated and stably maintained when certain histone-modifying enzymes were absent in G1-arrested cells. Ultimately, that study concluded that silencing establishment occurs through a shift in the landscape of histone modifications at *HML* and *HMR*, and that cells that do not fully experience this shift can maintain a partially silenced state. In this view, the intermediate silencing state observed in *sir2-G436D* may reflect a partial deficiency in its ability to deacetylate H4K16. It is interesting to note that deletion of *SAS2*, which is responsible for acetylation of H4K16, also exhibits intermediate silencing states at *HML* and *HMR* at the single-cell level (Xu *et al.* 2006). Notably, the intermediate silencing state in *sas2*Δ is not a bona fide epigenetic state, as it is present in all cells of that genotype. Taken together, these results strongly suggest that defects in different histone-modifying enzymes can exhibit similar phenotypes of intermediate silencing. This trend points to the existence of silencing intermediates that can be uncovered by modulating a complex landscape of histone modifications. The concept that histone modifications can tune transcription is broadly relevant, and the subject of studies like the modENCODE project, which classifies different chromatin landscapes and transcription profiles in *Drosophila melanogaster* and *C. elegans* (Gerstein *et al.* 2010; Kharchenko *et al.* 2011). Additional studies on *sir2-G436D*, *sas2*Δ, and other mutants will clarify how histone-modifying complexes can shift the strength of silencing and, in some cases, reveal heritable properties of heterochromatin.

Data availability

Strains and plasmids are available upon request. Supplemental files available at figshare: https://doi.org/10.25386/genetics.14176631.

Acknowledgments

We thank the members of our lab, especially Marc Fouet, for extensive discussions throughout the course of this work.

Funding

This work was funded by a SURF L&S Fellowship through UC Berkeley (to D.F.), by a National Science Foundation fellowship (DGE1752814 to D.S.S.), and by grants from the National Institutes of Health (GM31105, GM139488, and GM120374 to J.R.).

Conflicts of interest: The authors declare they have no competing interests in this work.

Literature cited

Bähler J, Wu J-Q, Longtine MS, Shah NG, Mckenzie A, III, *et al.* 1998. Heterologous modules for efficient and versatile PCR-based gene targeting in *Schizosaccharomyces pombe*. Yeast 14:943–951.

Brothers M, Rine J. 2019. Mutations in the PCNA DNA polymerase clamp of *Saccharomyces cerevisiae* reveal complexities of the cell cycle and ploidy on heterochromatin assembly. Genetics 213: 449–463.

Chien CT, Buck S, Sternglanz R, Shore D. 1993. Targeting of SIR1 protein establishes transcriptional silencing at HM loci and telomeres in yeast. Cell 75:531–541.

Dhillon N, Kamakaka RT. 2000. A Histone Variant, Htz1p, and a Sir1p-like Protein, Esc2p, Mediate Silencing at HMR. Mol Cell 6: 769–780.

Dodson AE, Rine J. 2015. Heritable capture of heterochromatin dynamics in *Saccharomyces cerevisiae*. Elife 4:e05007.

Ganley ARD, Ide S, Saka K, Kobayashi T. 2009. The effect of replication initiation on gene amplification in the rDNA and its relationship to aging. Mol Cell 35:683–693.

Gartenberg MR, Smith JS. 2016. The nuts and bolts of transcriptionally silent chromatin in *Saccharomyces cerevisiae*. Genetics 203: 1563–1599.

Gerstein MB, Lu ZJ, Nostrand ELV, Cheng C, Arshinoff BI, *et al.* 2010. Integrative analysis of the *Caenorhabditis elegans* genome by the modENCODE project. Science 330:1775–1787.

Gibbons JG, Branco AT, Godinho SA, Yu S, Lemos B. 2015. Concerted copy number variation balances ribosomal DNA dosage in human and mouse genomes. Proc Natl Acad Sci USA. 112: 2485–2490.

Goodnight D, Rine J. 2020. S-phase-independent silencing establishment in *Saccharomyces cerevisiae*. eLife 9:e58910.

Gottlieb S, Esposito RE. 1989. A new role for a yeast transcriptional silencer gene, SIR2, in regulation of recombination in ribosomal DNA. Cell 56:771–776.

Hall BE, Ellenberger TE. Unpublished. Crystal structure of the Sir2 deacetylase. 2HJH. doi: 10.2210/pdb2HJH/pdb

Hoppe GJ, Tanny JC, Rudner AD, Gerber SA, Danaie S, *et al.* 2002. Steps in assembly of silent chromatin in yeast: Sir3-independent binding of a Sir2/Sir4 complex to silencers and role for Sir2-dependent deacetylation. Mol Cell Biol. 22:4167–4180.

Hsu H-C, Wang C-L, Wang M, Yang N, Chen Z, *et al.* 2013. Structural basis for allosteric stimulation of Sir2 activity by Sir4 binding. Genes Dev. 27:64–73.

Iida T, Kobayashi T. 2019. RNA Polymerase I activators count and adjust Ribosomal RNA gene copy number. Mol Cell 73:645–654.e13.

Imai S, Armstrong CM, Kaeberlein M, Guarente L. 2000. Transcriptional silencing and longevity protein Sir2 is an NAD-dependent histone deacetylase. Nature 403:795–800.

Kaeberlein M, McVey M, Guarente L. 1999. The SIR2/3/4 complex and SIR2 alone promote longevity in *Saccharomyces cerevisiae* by two different mechanisms. Genes Dev. 13:2570–2580.

Kharchenko PV, Alekseyenko AA, Schwartz YB, Minoda A, Riddle NC, *et al.* 2011. Comprehensive analysis of the chromatin landscape in *Drosophila melanogaster*. Nature 471:480–485.

Kobayashi T, Ganley ARD. 2005. Recombination regulation by transcription-induced cohesin dissociation in rDNA repeats. Science 309:1581–1584.

Kobayashi T, Heck DJ, Nomura M, Horiuchi T. 1998. Expansion and contraction of ribosomal DNA repeats in *Saccharomyces cerevisiae*: requirement of replication fork blocking (Fob1) protein and the role of RNA polymerase I. Genes Dev. 12:3821–3830.

Kobayashi T, Horiuchi T. 1996. A yeast gene product, Fob1 protein, required for both replication fork blocking and recombinational hotspot activities. Genes Cells 1:465–474.

Kobayashi T, Horiuchi T, Tongaonkar P, Vu L, Nomura M. 2004. SIR2 regulates recombination between different rDNA repeats, but not

recombination within individual rRNA. Genes Yeast Cell 117: 441–453.

Kostriken R, Strathern JN, Klar AJS, Hicks JB, Heffron F. 1983. A site-specific endonuclease essential for mating-type switching in *Saccharomyces cerevisiae*. Cell 35:167–174.

Kueng S, Oppikofer M, Gasser SM. 2013. SIR proteins and the assembly of silent chromatin in budding yeast. Annu Rev Genet. 47: 275–306.

Landry J, Sutton A, Tafrov ST, Heller RC, Stebbins J, *et al.* 2000. The silencing protein SIR2 and its homologs are NAD-dependent protein deacetylases. Proc Natl Acad Sci USA. 97:5807–5811.

Lee ME, DeLoache WC, Cervantes B, Dueber JE. 2015. A highly characterized yeast toolkit for modular, multipart assembly. ACS Synth Biol. 4:975–986.

Lee TI, Young RA. 2013. Transcriptional regulation and its misregulation in disease. Cell 152:1237–1251.

Liu E, Hu Y. 2010. Construction of a xylose-fermenting *Saccharomyces cerevisiae* strain by combined approaches of genetic engineering, chemical mutagenesis and evolutionary adaptation. Biochem Eng J. 48:204–210.

Longtine MS, Iii AM, Demarini DJ, Shah NG, Wach A, *et al.* 1998. Additional modules for versatile and economical PCR-based gene deletion and modification in *Saccharomyces cerevisiae*. Yeast 14: 953–961.

Lu AX, Zarin T, Hsu IS, Moses AM. 2019. YeastSpotter: accurate and parameter-free web segmentation for microscopy images of yeast cells. Bioinformatics 35:4525–4527.

Lyckegaard EM, Clark AG. 1989. Ribosomal DNA and stellate gene copy number variation on the Y chromosome of *Drosophila melanogaster*. Proc Natl Acad Sci USA. 86:1944–1948.

Merker RJ, Klein HL. 2002. *hpr1Δ* affects ribosomal DNA recombination and cell life span in *Saccharomyces cerevisiae*. Mol Cell Biol. 22: 421–429.

Michel AH, Kornmann B, Dubrana K, Shore D. 2005. Spontaneous rDNA copy number variation modulates Sir2 levels and epigenetic gene silencing. Genes Dev. 19:1199–1210.

Moazed D, Johnson AD. 1996. A deubiquitinating enzyme interacts with SIR4 and regulates silencing in S. *cerevisiae*. Cell 86:667–677.

Pillus L, Rine J. 1989. Epigenetic inheritance of transcriptional states in S. *cerevisiae*. Cell 59:637–647.

Rine J, Herskowitz I. 1987. Four genes responsible for a position effect on expression from *HML* and *HMR* in *Saccharomyces cerevisiae*. Genetics 116:9–22.

Rine J, Strathern JN, Hicks JB, Herskowitz I. 1979. A suppressor of mating-type locus mutations in *Saccharomyces cerevisiae*: evidence for and identification of cryptic mating-type loci. Genetics 93: 877–901.

Rusché LN, Kirchmaier AL, Rine J. 2002. Ordered nucleation and spreading of silenced chromatin in *Saccharomyces cerevisiae*. Mol Biol Cell 13:2207–2222.

Saxton DS, Rine J. 2019. Epigenetic memory independent of symmetric histone inheritance. eLife 8:585.

Schindelin J, Arganda-Carreras I, Frise E, Kaynig V, Longair M, *et al.* 2012. Fiji: an open-source platform for biological-image analysis. Nat Methods 9:676–682.

Sherman JM, Stone EM, Freeman-Cook LL, Brachmann CB, Boeke JD, *et al.* 1999. The conserved core of a human SIR2 homologue functions in yeast silencing. Mol Biol Cell 10:3045–3059.

Stone EM, Reifsnyder C, McVey M, Gazo B, Pillus L. 2000. Two classes of *sir3* mutants enhance the *sir1* mutant mating defect and abolish telomeric silencing in *Saccharomyces cerevisiae*. Genetics 155: 509–522.

Straight AF, Shou W, Dowd GJ, Turck CW, Deshaies RJ, *et al.* 1999. Net1, a Sir2-associated nucleolar protein required for rDNA silencing and nucleolar integrity. Cell 97:245–256.

Thurtle DM, Rine J. 2014. The molecular topography of silenced chromatin in *Saccharomyces cerevisiae*. Genes Dev. 28:245–258.

Winston F. 2008. EMS and UV Mutagenesis in Yeast. Curr Protoc Mol Biol. 82:13.10.1002/0471142727.mb1303bs82

Xu EY, Zawadzki KA, Broach JR. 2006. Single-cell observations reveal intermediate transcriptional silencing states. Mol Cell 23: 219–229.

Zhang QF, Maroof MAS, Allard RW. 1990. Effects on adaptedness of variations in ribosomal DNA copy number in populations of wild barley (*Hordeum vulgare ssp. spontaneum*). Proc Natl Acad Sci USA. 87:8741–8745.

Communicating editor: A. Mitchell